

SISSA 78/2003/EP
 SINP/TNP/03-32
 hep-ph/0309174

Constraints on neutrino oscillation parameters from the SNO salt phase data

Abhijit Bandyopadhyay¹, Sandhya Choubey^{2,3}, Srubabati Goswami^{4,5}, S.T. Petcov^{3,2,6}, D.P. Roy⁷

¹*Saha Institute of Nuclear Physics, 1/AF, Bidhannagar, Calcutta 700 064, India,*

²*INFN, Sezione di Trieste, Trieste, Italy,*

³*Scuola Internazionale Superiore di Studi Avanzati, I-34014, Trieste, Italy,*

⁴*Harish-Chandra Research Institute, Chhatnag Road, Jhusi, Allahabad 211 019, India,*

⁵*The Abdus Salam International Centre for Theoretical Physics, I-34100, Trieste, Italy,*

⁶*Institute of Nuclear Research and Nuclear Energy, Bulgarian Academy of Science, Sofia, Bulgaria,*

⁷*Tata Institute of Fundamental Research, Homi Bhabha Road, Mumbai 400 005, India*

Abstract

The physics implications of the just published salt phase data from the SNO experiment are examined. The effect of these data on the allowed ranges of the solar neutrino oscillation parameters, Δm_{21}^2 and $\sin^2 \theta_{12}$, are studied in the cases of two- and three- neutrino mixing. In the latter case we derive an upper limit on the angle θ_{13} . Constraints on the solar ν_e transitions into a mixture of active and sterile neutrinos are also presented. Finally, we give predictions for the day-night asymmetry in the SNO experiment, for the event rate in the BOREXINO and LowNu experiments, and discuss briefly the constraints on the solar neutrino oscillation parameters which can be obtained with prospective KamLAND data.

1 Introduction

The past two years have witnessed remarkable experimental progress in the studies of neutrino mixing and oscillations. The latest addition to this magnificent effort is the salt phase data from the SNO experiment [1].

In 2001, the evidences for solar neutrino oscillations obtained in the pioneer experiment of Davis et al. (Homestake) and in the Kamiokande, SAGE, GALLEX/GNO [2] and Super-Kamiokande [3] experiments, were reinforced by the first results of the SNO experiment on the charged current (CC) reaction on deuterium induced by solar neutrinos [4]. In conjunction with the Super-Kamiokande (SK) $\nu - e^-$ scattering data, the SNO CC data established the existence of solar ν_e flavour conversion with a statistical significance of 3.3 s.d.. This conclusion was further corroborated by the 2002 SNO data on the neutral current (NC) reaction on deuterium, caused by solar neutrinos [5]. The combined CC and NC SNO data showed the presence at 5.3 s.d. of a nonzero $\nu_{\mu,\tau}$ and/or $\bar{\nu}_{\mu,\tau}$ component in the flux of the solar 8B neutrinos reaching the Earth. At each stage, the SNO data enabled one to determine with improved precision the average solar ν_e survival probability P_{ee} from the CC reaction data, and the 8B flux normalisation f_B from the data on the NC reaction. This in turn led to a diminishing of the allowed regions of values of the two parameters - the neutrino mass squared difference Δm_{21}^2 ($\equiv \Delta m_{\odot}^2$) and the mixing angle θ_{12} ($\equiv \theta_{\odot}$), characterizing the solar neutrino oscillations. The SNO CC data had the main impact of ruling out the Small Mixing Angle (SMA) MSW [6] region in conjunction with the SK data [4, 7]. The SNO data from the D_2O phase¹ clearly showed preference for the Large Mixing Angle (LMA) MSW solution of the solar neutrino problem, disfavoring the small mixing angle (SMA) MSW and the relatively low Δm_{21}^2 (LOW, QVO) solutions [5, 8]. The first results of the KamLAND experiment [9], under the plausible assumption of CPT-invariance in the lepton sector, established the LMA solution as unique solution of the solar neutrino problem. All other solutions were reduced to play at most a minor role in the solar ν_e transitions.

The combined two-neutrino oscillation analyses of the solar neutrino and KamLAND data, available before the publication of the SNO salt phase results, identified two distinct solution sub-regions within the LMA solution region (see, e.g., [10, 11]). For the best fit values of Δm_{\odot}^2 and θ_{\odot} in the two sub-regions - low-LMA and high-LMA, it was found in [10], respectively: $\Delta m_{\odot}^2 = 7.2 \times 10^{-5} \text{ eV}^2$, $\sin^2 \theta_{\odot} = 0.3$, and $\Delta m_{\odot}^2 = 1.5 \times 10^{-4} \text{ eV}^2$, $\sin^2 \theta_{\odot} = 0.3$. The low-LMA solution was preferred statistically by the data. At 99.73% C.L. one obtained [10]:

$$\Delta m_{\odot}^2 \cong (5.0 - 20.0) \times 10^{-5} \text{ eV}^2, \quad \sin^2 \theta_{\odot} \cong (0.21 - 0.47) . \quad (1)$$

In the case of 3-neutrino mixing, the analysis of the solar neutrino and KamLAND data involves an additional parameter θ_{13} - the neutrino mixing angle limited by the CHOOZ and Palo Verde experiments [12]. The precise upper limit on $\sin^2 \theta_{13}$ depends on the value of Δm_{31}^2 - the neutrino mass squared difference responsible for the atmospheric ν_{μ} and $\bar{\nu}_{\mu}$ oscillations (see, e.g., [13]). The preliminary results of an improved analysis of the SK atmospheric neutrino data, performed

¹Here, and in the rest of the the paper, by D_2O phase we mean the NC reactions due to the final state neutron capture on deuterium.

Data set used	best-fit parameters		99% C.L. allowed range	
	$\Delta m_{21}^2 / (10^{-5} \text{eV}^2)$	$\sin^2 \theta_{12}$	$\Delta m_{21}^2 / (10^{-5} \text{eV}^2)$	$\sin^2 \theta_{12}$
Cl+Ga+SK+ D_2O	6.06	0.29	3.2 – 24.5	0.21 – 0.44
Cl+Ga+SK+salt	6.08	0.28	3.0 – 23.7	0.19 – 0.43
Cl+Ga+SK+ D_2O +salt	6.06	0.29	3.2 – 17.2	0.22 – 0.40
Cl+Ga+SK+ D_2O +KL	7.17	0.3	5.3 – 9.9	0.22 – 0.44
Cl+Ga+SK+ D_2O +salt+KL	7.17	0.3	5.3 – 9.8	0.22 – 0.40

Table 1: The best-fit values of the solar neutrino oscillation parameters, obtained using different combinations of data sets. Shown also are the 99% C.L. (corresponding to $\Delta\chi^2$ for 2 parameters) allowed ranges of the parameters from the different analyses.

recently by the SK collaboration, gave [14]

$$1.3 \times 10^{-3} \text{eV}^2 \lesssim \Delta m_{31}^2 \lesssim 3.1 \times 10^{-3} \text{eV}^2, \quad 90\% \text{ C.L.}, \quad (2)$$

with a best fit value $\Delta m_{31}^2 = 2.0 \times 10^{-3} \text{eV}^2$.

After the KamLAND results the two major issues to be settled with the future data are:

- Resolving the ambiguity between the low-LMA and the high-LMA solutions and thereby obtaining tighter constraints on Δm_{21}^2 .
- Constraining further the allowed range of the solar neutrino mixing angle, θ_{12} .

In the present article we examine some of the physics implications of the latest salt phase data from SNO [1]. We study, in particular, the effect of these data on the allowed ranges of the solar neutrino oscillation parameters, Δm_{21}^2 and $\sin^2 \theta_{12}$. This is done in the cases of two- and three-neutrino mixing. In the latter case we derive an upper limit on the angle θ_{13} . Constraints on the solar ν_e transitions into a mixture of active and sterile neutrinos, i.e., on the allowed sterile fraction, are also presented. Finally, we give predictions for the day-night asymmetry in the SNO experiment, for the event rate in the BOREXINO and LowNu experiments, and discuss briefly the constraints on the solar neutrino oscillation parameters which can be obtained with prospective KamLAND data.

2 Two generation oscillation analysis

2.1 Analysis with global solar neutrino data

In this Section we first perform a two generation oscillation analysis of the global solar data, incorporating the new SNO results. We include the total rates from the radiochemical experiments Cl and Ga (Gallex, SAGE and GNO combined) [2] and the 1496 day 44 bin SK Zenith angle

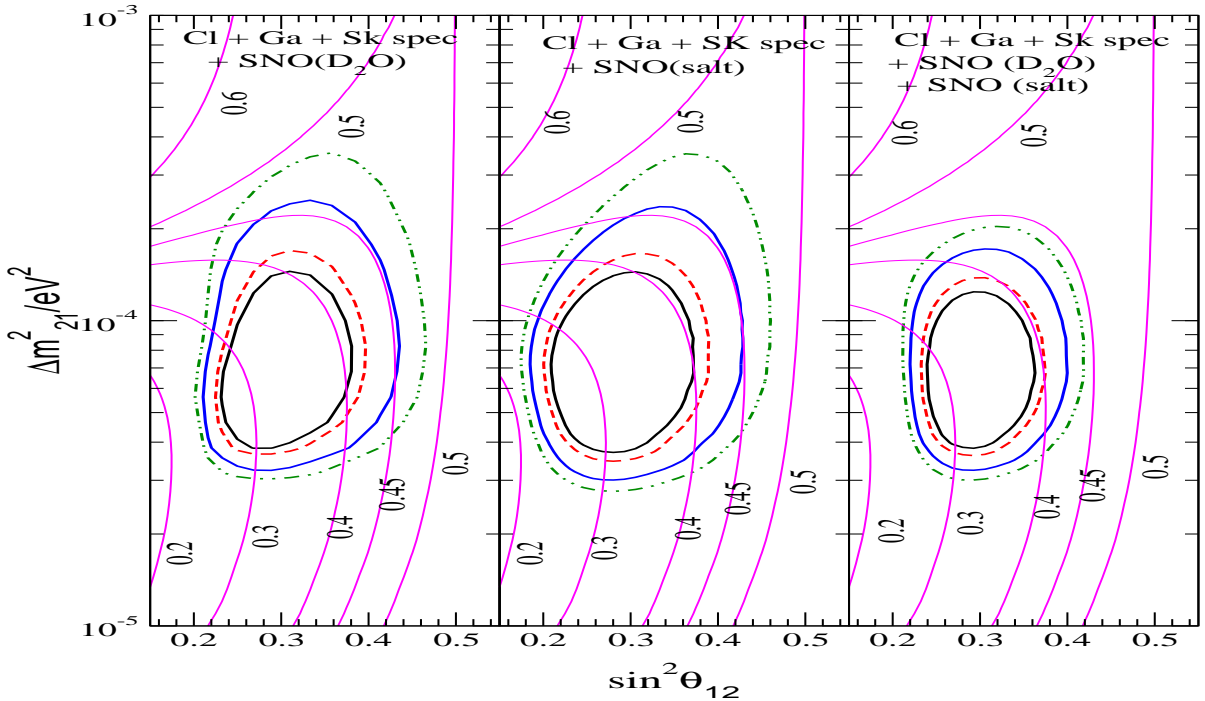


Figure 1: The 90%, 95%, 99% and 99.73% C.L. allowed areas in the Δm_{21}^2 – $\sin^2 \theta_{12}$ plane from global χ^2 -analysis of data from solar neutrino experiments. We use the two parameter $\Delta \chi^2$ values to plot the C.L. contours. Also shown are the lines of constant CC/NC ratio $R_{CC/NC}$.

spectrum data [3]². For SNO we take the combined CC, NC and Electron Scattering (ES) 34 bin energy spectrum data from their D_2O phase [5], and the recently reported CC, NC and ES rates from the latest salt phase of the experiment [1]³. To ascertain the impact of the salt data and facilitate comparison between different phases we include the SNO data in three following ways in our analysis.

1. Consider only the CC+ES+NC day/night spectra from the D_2O phase
2. Consider only the CC, ES and NC rates from the salt phase

²SK has recently reanalyzed their day/night data with improved precision [15]. However, the information content in [15] is not enough for including it in our analysis.

³Note that the salt enriched data from SNO gives the CC,ES and NC total rates without any assumption on the 8B spectrum shape.

3. Consider data from both phases together

We follow the instructions given in [16] by the SNO Collaboration to treat the SNO data.

For our statistical analysis of the global solar neutrino data we follow a covariant approach and minimise the χ^2 defined as

$$\chi_{\odot}^2 = \sum_{i,j=1}^N (R_i^{\text{expt}} - R_i^{\text{theory}})(\sigma_{ij}^2)^{-1}(R_j^{\text{expt}} - R_j^{\text{theory}}) \quad (3)$$

where R_i are the solar data points, N is the number of data points and $(\sigma_{ij}^2)^{-1}$ is the inverse of the covariance matrix, containing the squares of the correlated and uncorrelated experimental and theoretical errors. We leave the 8B flux normalisation factor f_B to vary freely in our analysis. For further details of our solar analysis we refer the reader to [7, 8].

The results of our analysis of the global solar neutrino data are presented in Table 1 and Figure 1. Table 1 gives the best-fit points and the allowed range of parameter values obtained from the analysis. The best-fit for the global analysis, including the complete SNO data from both phases, is obtained at $\Delta m_{21}^2 = 6.06 \times 10^{-5} \text{ eV}^2$, $\sin^2 \theta_{12} = 0.29$ and $f_B = 1.04$. Note that if we consider only the salt phase data from SNO, the best-fit $\sin^2 \theta_{12}$ is marginally lower.

In the first panel of Figure 1 we show the allowed area in the parameter space when only the spectrum data from the D_2O phase is included. In the second panel we show the allowed areas including the SNO salt data but excluding the SNO spectrum data from the D_2O phase. A comparison of the first two panels shows that with the exclusion of the D_2O phase spectrum data, the allowed region enlarges in size. Even though the D_2O phase of the SNO data agrees remarkably well with the salt phase, the ratio of CC and NC events is slightly different for the two phases. In particular, for the D_2O phase, if one uses the data given by SNO for the null hypothesis, the ratio of the CC to NC event rates, $R_{CC/NC} = 0.346$. For the salt phase the ratio is $R_{CC/NC} = 0.306$. Thus, the CC to NC ratio has decreased. In Figure 1 we have also superimposed on the allowed regions the iso- $R_{CC/NC}$ contour lines [17]. We clearly see that since the $R_{CC/NC}$ for the salt phase is lower, the allowed regions shift left, following the iso- $R_{CC/NC}$ contours. This results in the shift of the allowed range of $\sin^2 \theta_{12}$ to slightly lower values (see Table 1). The allowed Δm_{21}^2 shift to slightly lower values for the same reason.

The third panel shows the allowed areas including the SNO data from both D_2O phase as well as the salt phase. Following the SNO collaboration [16], we treat these two phases as separate experiments with no correlation between them. Combination of the salt phase and the D_2O phase data produce a more restrictive upper bound on $\Delta m_{21}^2 \leq 1.7 \times 10^{-4} \text{ eV}^2$ (99.73% C.L.). The upper limit on $\sin^2 \theta_{12}$ also improves compared to what we have before the salt phase data, as can be seen by comparing the first panel with the last one in Figure 1. The exact values of the ranges are given in Table 1.

2.2 Constraints from combined solar and KamLAND data

We next include the 162 ton-year first results from the KamLAND experiment into our analysis. For KamLAND we use the 13 bin spectrum data and defined a χ^2 assuming a Poissonian

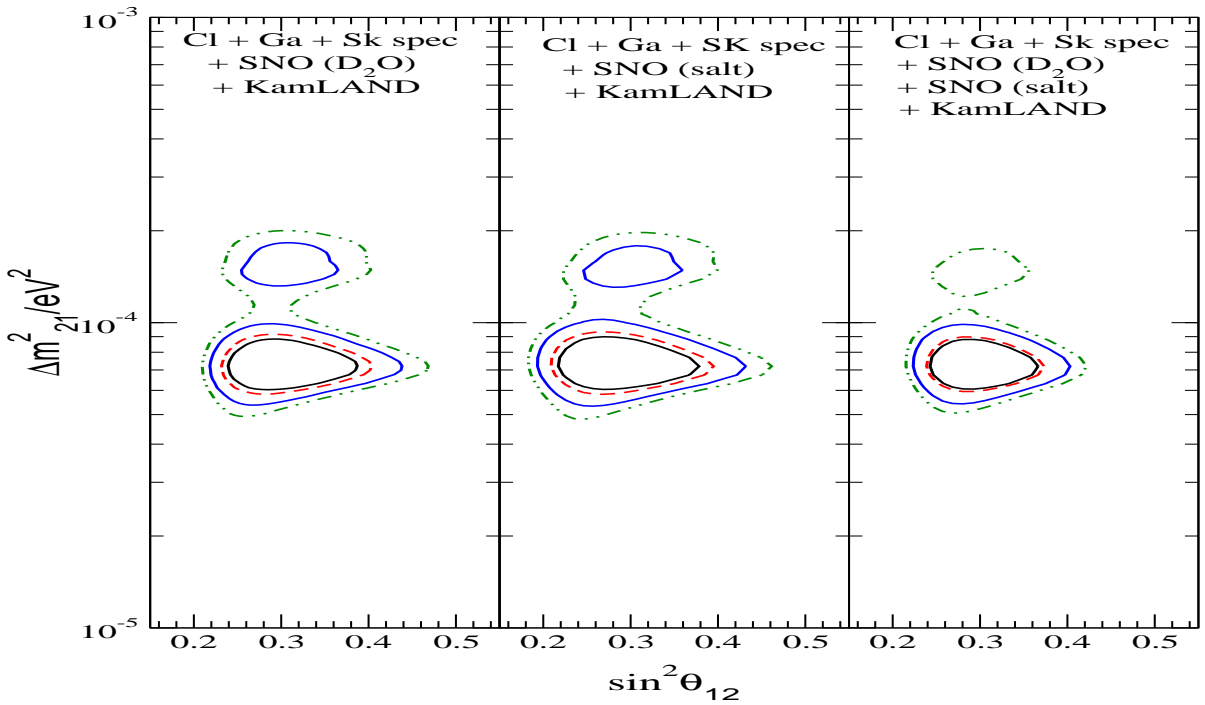


Figure 2: The 90%, 95%, 99% and 99.73% C.L. allowed areas in the Δm_{21}^2 – $\sin^2 \theta_{12}$ plane from global χ^2 -analysis of solar and KamLAND data. We use the two parameter $\Delta\chi^2$ values to plot the C.L. contours.

distribution as

$$\chi_{klspc}^2 = \sum_i \left[2(X_n S_{KL,i}^{theory} - S_{KL,i}^{expt}) + 2S_{KL,i}^{expt} \ln\left(\frac{S_{KL,i}^{expt}}{X_n S_{KL,i}^{theory}}\right) \right] + \frac{(X_n - 1)^2}{\sigma_{sys}^2} \quad (4)$$

where σ_{sys} is taken to be 6.42% and X_n allowed to vary freely (see [10] for the details of the analysis). In the last 2 rows of Table 1 we give the best-fit data points and the allowed ranges of the parameters obtained before and after including the latest salt phase SNO data into the global analysis. The best-fit for the combined global analysis comes in the low-LMA region at $\Delta m_{21}^2 = 7.17 \times 10^{-5}$ eV² and $\sin^2 \theta_{12} = 0.30$. Thus, the best-fit values of the parameters for the combined solar+KamLAND analysis do not change after inclusion of the latest SNO results. The best-fit $f_B = 1.02$.

In figure 2 we present the corresponding allowed regions. Again we present our results separately for only the D_2O phase (left-hand panel), only the salt phase (middle panel) and the global

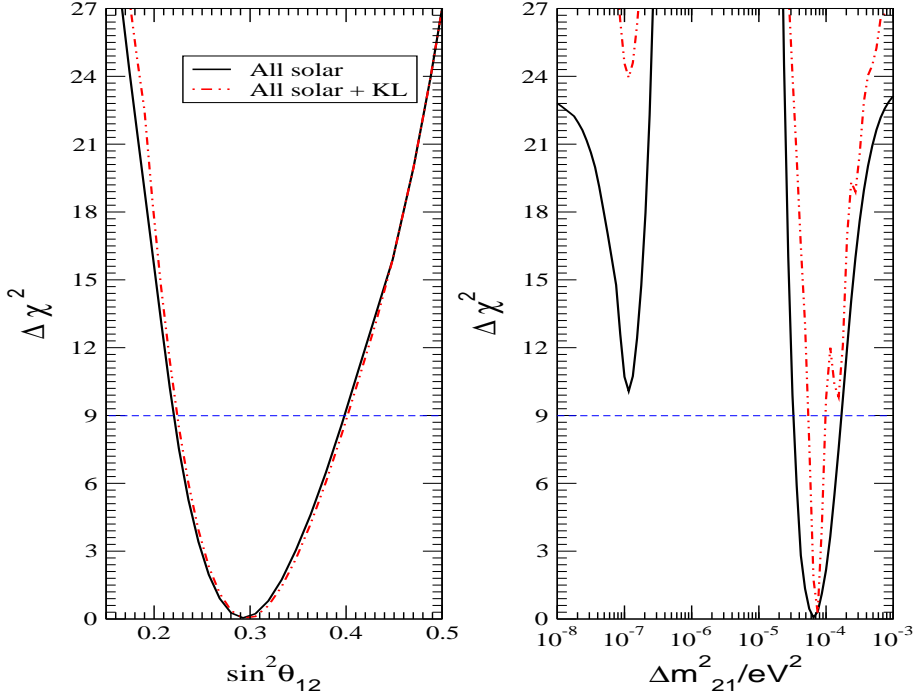


Figure 3: Bounds on Δm_{21}^2 and $\sin^2 \theta_{12}$ from the $\Delta\chi^2$ as a function of Δm_{21}^2 and $\sin^2 \theta_{12}$ respectively. In both panels all the other parameters are allowed to vary freely. The dashed line shows the 3σ limit corresponding to one d.o.f.

data with the two phases combined (right-hand panel). Note the shift of the allowed areas for the middle panel which includes only the salt phase data to lower values of $\sin^2 \theta_{12}$. We find that although the separate inclusion of the data from each phase allows the high-LMA region at 99% C.L. a combination of both allows the high-LMA region only at 3σ .

In Figure 3 we show the dependence of $\Delta\chi^2 = \chi^2 - \chi^2_{min}$ to Δm_{21}^2 (right-hand panel) and $\sin^2 \theta_{12}$ (left-hand panel) respectively, after marginalising over the remaining free parameters. The solid lines show the $\Delta\chi^2$ for the global solar neutrino data, while the dashed curves correspond to the combined solar and KamLAND data. We note that the Δm_{21}^2 corresponding to the LOW solution is ruled out at slightly more than 3σ by the solar neutrino data alone, and at nearly 5σ from the combined solar and KamLAND data. KamLAND results are seen to produce a remarkable constraint on Δm_{21}^2 . Maximal mixing is now ruled out at more the 5σ level by the solar data alone. The KamLAND data does not put a strong constraint on $\sin^2 \theta_{12}$.

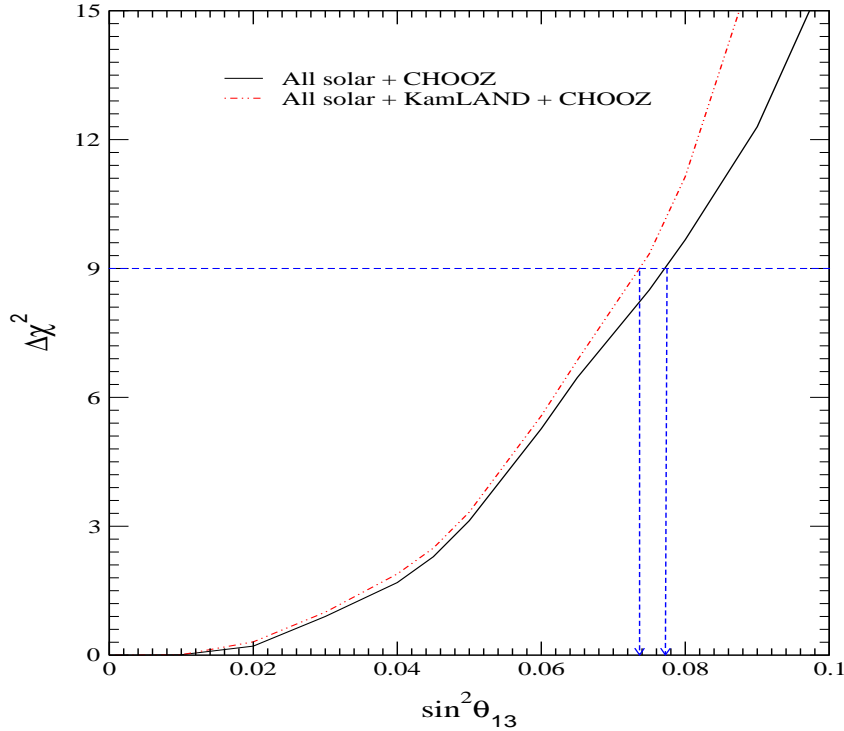


Figure 4: Bounds on the mixing angle θ_{13} from the global solar neutrino data and CHOOZ (solid line) and the combined solar, CHOOZ and KamLAND data (dashed line). All the other parameters are allowed to vary freely. The dashed line shows the 3σ limit corresponding to one parameter.

3 Bounds from three-neutrino oscillation analysis

So far we have presented results obtained in the framework of two-neutrino oscillations, where the solar ν_e oscillates into another active neutrino with a different flavor. However, if the mixing angle θ_{13} which is restricted by the CHOOZ and Palo Verde data, is not zero, there will be some transition also to the third heaviest neutrino mass eigenstate, driven by Δm_{31}^2 . The relevant electron neutrino/antineutrino survival probability in the three-neutrino mixing case is given by the following expression:

$$P_{ee}^{3gen} = \cos^4 \theta_{13} P_{ee}^{2gen} + \sin^4 \theta_{13} \quad (5)$$

where P_{ee}^{2gen} is the ν_e survival probability for two-neutrino mixing [18]. Since $\sin^4 \theta_{13}$ can be neglected to a good approximation, and since for the solar neutrinos $P_{ee}^{2gen} \approx \sin^2 \theta_{12}$ in the low-

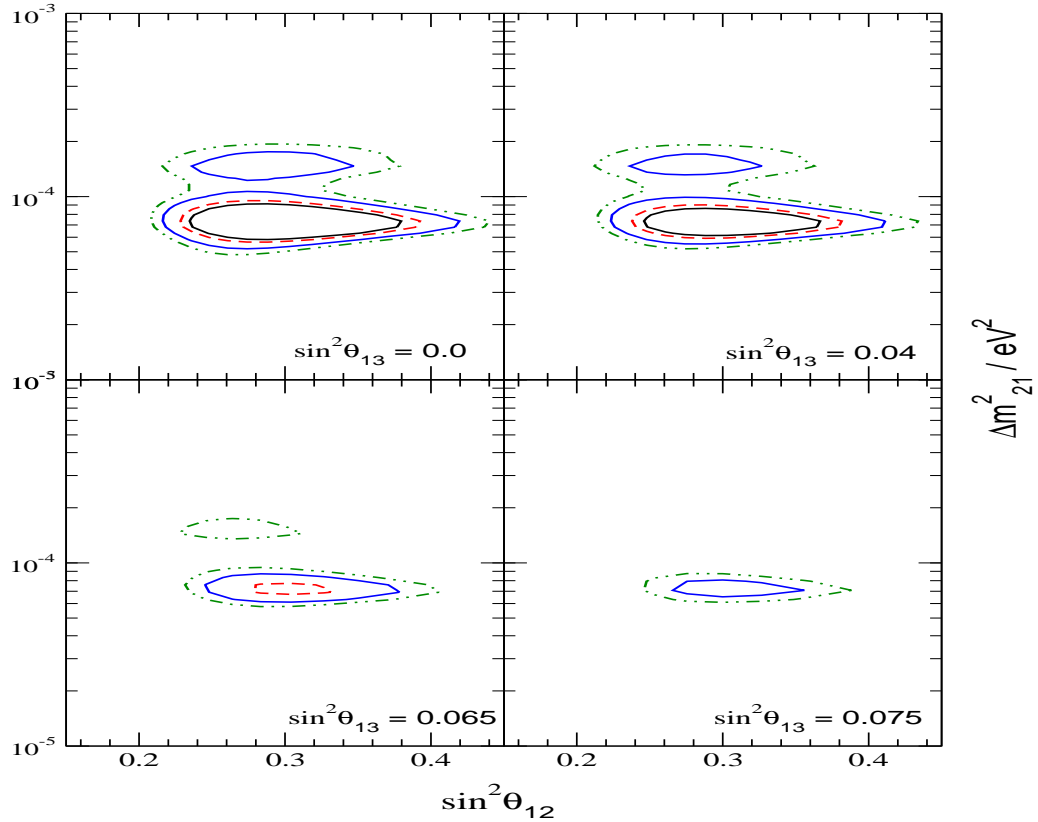


Figure 5: The 90%, 95%, 99% and 99.73% C.L. allowed contours in the $\Delta m_{21}^2 - \sin^2 \theta_{12}$ plane, from the three generation analysis of the global solar and reactor data, including KamLAND and CHOOZ. The different panels are drawn at different fixed values of $\sin^2 \theta_{13}$. Here we use the three parameter $\Delta\chi^2$ values to plot the C.L. contours.

LMA region, one has $P_{ee}^{3gen} \approx \cos^4 \theta_{13} \sin^2 \theta_{12}$. For the KamLAND reactor antineutrinos the matter effects are negligible and one gets $P_{ee}^{3gen} = \cos^4 \theta_{13} \{1 - \sin^2 2\theta_{12} \sin^2(\Delta m_{21}^2 L/4E)\}$, where L is the source-detector distance and E the antineutrino energy. From Eq. (5), we note that the presence of a non-zero θ_{13} shifts θ_{12} , obtained from the solar neutrino data analysis, to larger values. On the contrary, for the reactor antineutrinos, we should expect the allowed range of θ_{12} to shift to smaller values, if θ_{13} is non-zero and sufficiently large. The survival probability for the short-baseline CHOOZ experiment is approximately given by $P_{ee}^{3gen} \approx 1 - \sin^2 2\theta_{13} \sin^2(\Delta m_{31}^2 L/4E)$ and is hence very sensitive to the range of allowed value of atmospheric neutrino mass squared difference Δm_{31}^2 . We use the 3σ allowed value of Δm_{31}^2 from the latest SK analysis of the atmospheric neutrino data [14]. We perform a combined three neutrino oscillation analysis of the global solar neutrino data and reactor data, including both the KamLAND and CHOOZ results.

In Figure 4 we present the $\Delta\chi^2$ obtained for various fixed values of the $\sin^2\theta_{13}$, when all other parameters are allowed to vary freely. The 3σ bounds on $\sin^2\theta_{13}$, from the global solar neutrino analysis can be directly read from the figure as $\sin^2\theta_{13} < 0.077$. For the combined analysis with solar and KamLAND data, the bound marginally tightens to $\sin^2\theta_{13} < 0.074$. We have checked that the bounds on Δm_{21}^2 and $\sin^2\theta_{12}$, even for the three-generation analysis, are the same as those given in Figure 3.

In Figure 5 we present the allowed regions in the $\Delta m_{21}^2 - \sin^2\theta_{12}$ parameter space, for four fixed values of θ_{13} . The presence of a small non-zero θ_{13} improves the fit in the regions of the parameter space with higher values of Δm_{21}^2 , e.g., in the high-LMA zone, where the 8B neutrino transitions are not affected by matter effects over the entire energy spectrum, and which therefore give a larger value of CC/NC ratio [17]. The presence of the $\cos^4\theta_{13}$ factor in the survival probability acts as a normalisation which effectively reduces the CC event rate and hence makes the high-LMA zone less disfavored by the data. Since matter effects in the Sun are relatively small for the high-LMA values of Δm_{21}^2 , the allowed regions in these zones appear at smaller values of θ_{12} , as discussed above. However, as θ_{13} increases, the allowed areas shrink and finally vanish beyond $\sin^2\theta_{13} > 0.075$. Note that we get allowed areas at $\sin^2\theta_{13} = 0.075$ even though from Figure 4 the 3σ range appears to be $\sin^2\theta_{13} < 0.074$ since in Figure 5 we use a $\Delta\chi^2$ which corresponds to a three parameter fit.

4 Constraints on transitions into a state with a sterile neutrino component

As is well known, the explanation of the positive evidence of oscillation from the LSND [19] experiment and the solar and atmospheric neutrino oscillation data requires the existence of a fourth neutrino which has to be inert. A comparison of the SNO CC and NC data from the D_2O phase had already ruled out solar ν_e oscillations into pure sterile state at 5.3 s.d. [5]. The inclusion of the SNO salt data raises the degree of disfavour to 7.8σ level [1]. However, transitions to “mixed” states, where the final neutrino state is a mixture of active and sterile components, is still allowed by the data. We find the limits on the sterile fraction from the global data.

We consider a general case where the ν_e produced in the sun transforms into a “mixed” state given by $\nu' = \sin\alpha \nu_{active} + \cos\alpha \nu_{sterile}$. Thus, $\sin^2\alpha (\cos^2\alpha)$ gives the fraction of the active(sterile) component in the resultant solar neutrino flux at earth. In Figure 6 we present the plots of $\Delta\chi^2$ vs f_B (left-hand panel) and $\Delta\chi^2$ vs $\sin^2\alpha$ (right-hand panel) allowing the mass and mixing parameters to vary freely in the LMA region. The solid lines give the constraints from the solar data alone, while the dashed lines correspond to the combined solar and KamLAND data. The range of allowed values of f_B at 3σ is $0.87 - 1.2(1.16)$ from the global solar(solar+KamLAND) data. The fraction of allowed value for the sterile fraction in the resultant solar neutrino beam is given by $1 - \sin^2\alpha < 0.6(0.52)$ at 3σ from the solar(solar+KamLAND) data. Before the salt data was declared, the corresponding limit for the sterile fraction at 3σ from the combined solar+KamLAND analysis was $1 - \sin^2\alpha < 0.54$. Thus the salt data is seen to only marginally tighten the noose on the possible presence of a sterile component in the solar neutrino flux.

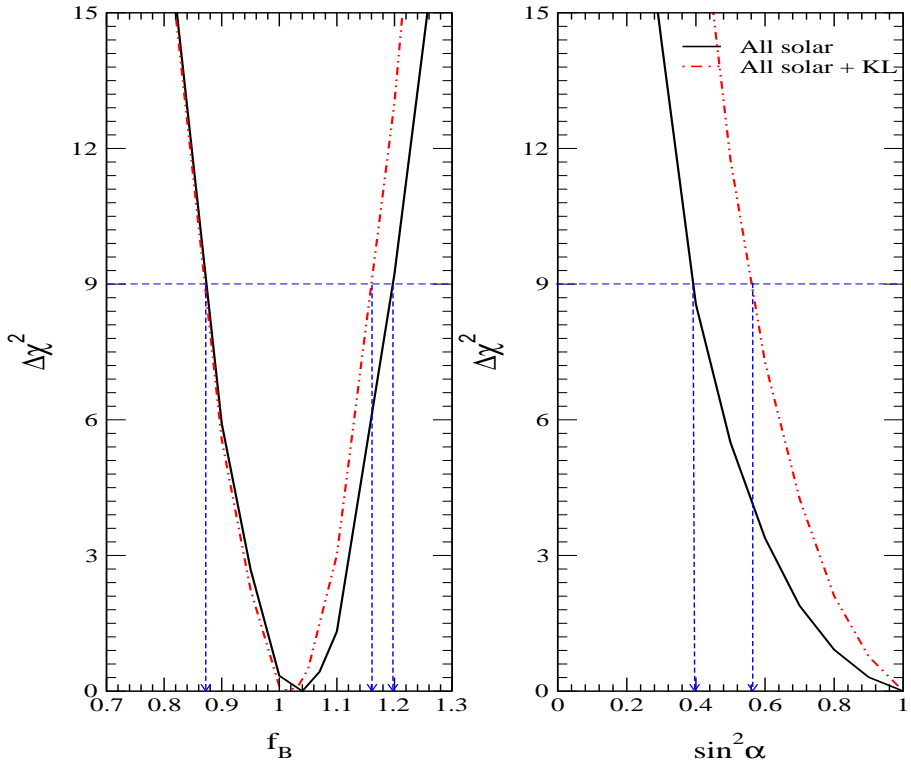


Figure 6: Bounds on f_B and the sterile fraction in the solar neutrino flux, given by $1 - \sin^2 \alpha$. The left panel shows the $\Delta\chi^2$ as a function of f_B , while the right-hand panel gives the corresponding bounds on $\sin^2 \alpha$. The $\Delta\chi^2$ is marginalised over all the oscillation parameters. The dashed line shows the 3σ limit corresponding to one parameter.

5 Future and outlook

With the latest salt phase data from SNO giving further credence to the low-LMA solution, the stage is set for the precision era in the field of solar neutrino physics. The spurious high-LMA solution stands disfavored and only a small area appears at 3σ level. The next phase of the SNO experiment will be devoted to obtaining neutral current data using Helium counters [20]. This would give a totally uncorrelated information on the CC and NC event rates observed at SNO. In the near future SNO is expected to provide data on the day/night spectrum, which could be used in a statistical analysis to further constrain the solar neutrino oscillation parameters [16]. One of the related observables is the day-night asymmetry:

$$A_{DN} = 2 \frac{N - D}{N + D}. \quad (6)$$

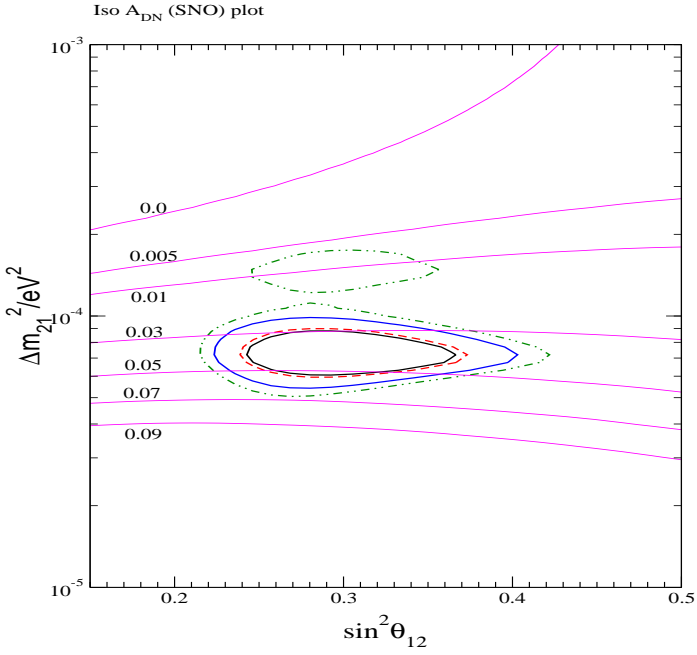


Figure 7: Lines of constant day-night asymmetry for the SNO experiment, superposed on the allowed region from the global analysis of the solar and KamLAND data.

The predicted A_{DN} in SNO, for the current best-fit values of the parameters in the low-LMA region, as well as the corresponding 3σ range, are given by:

$$A_{DN}^{SNO} = 0.04, \quad (3\sigma \text{ range} \equiv 0.02 - 0.07); \quad \text{low - LMA} \quad (7)$$

For the barely allowed high-LMA solution we get:

$$A_{DN}^{SNO} = 0.01, \quad (3\sigma \text{ range} \equiv 0.007 - 0.02); \quad \text{high - LMA} \quad (8)$$

In Figure 7 we show the lines of constant A_{DN} for SNO [17].

The potential of Borexino [21] and any generic electron scattering experiment for the low energy pp neutrinos – the LowNu experiments [22] – in constraining the mass and mixing parameters have been studied most recently in [23, 24]. The predicted rates for Borexino and LowNu experiments are

$$R_{Be} = 0.65, \quad (3\sigma \text{ range} \equiv 0.61 - 0.71); \quad \text{low - LMA} \quad (9)$$

$$R_{pp} = 0.71, \quad (3\sigma \text{ range} \equiv 0.67 - 0.76); \quad \text{low - LMA} \quad (10)$$

However we expect the best precision measurement results from the reactor experiment KamLAND [25, 26]. With 1 kTy statistics in KamLAND data we might expect to reduce the uncertainty in the Δm_{21}^2 determination to a few percent [10, 23]. In Figure 8 we present the two-generation allowed areas in the solar neutrino parameter space from a combined analysis using the

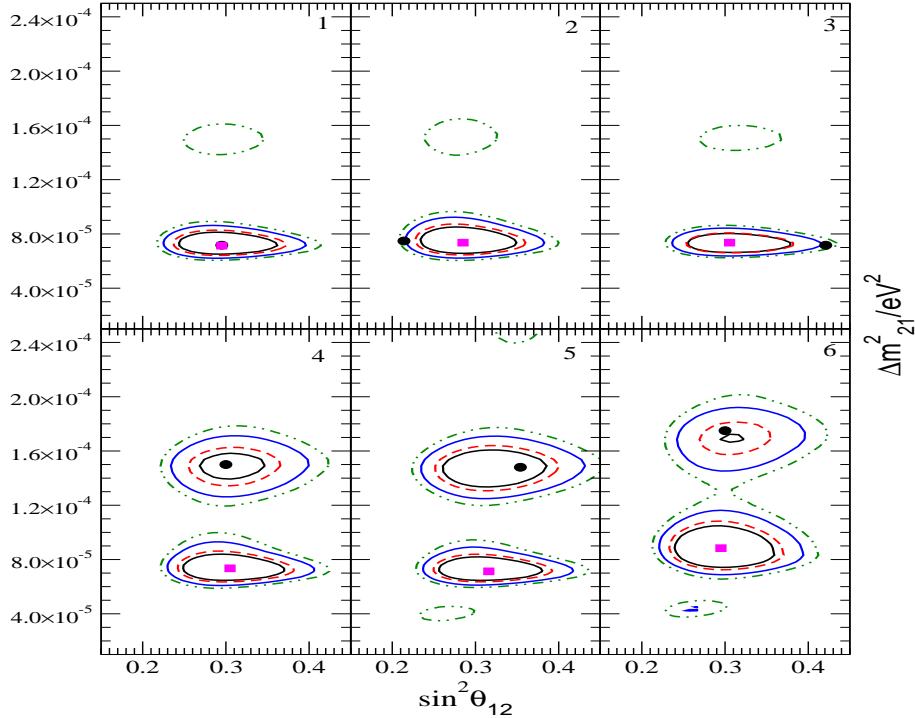


Figure 8: The 90%, 95%, 99% and 99.73% C.L. allowed regions obtained from a combined analysis using the global solar neutrino data and a prospective 1 kTy simulated KamLAND data. The points in the parameter space, for which the 1 kTy KamLAND data has been simulated, are shown by the black dots; they have been chosen to lie within the current 3σ allowed regions. The best-fit point of the combined analysis are shown as red “boxes”.

current global solar neutrino data and a future prospective 1 kTy simulated data in KamLAND. Since in future the systematic uncertainty in KamLAND is expected to reduce specially with the fiducial volume calibration we use a value of 5% for the KamLAND systematic error in this analysis. The black dots in the various panels of Figure 8 denote the point in the parameter space for which the data has been simulated. The pink squares give the point where we get the best-fit for the joint analysis. For the first row of panels, the points at which we simulate the KamLAND data lie in the low-LMA zone. We can note that if the true solution lies in the low-LMA band, then the spurious high-LMA still appears at the 3σ level, though the allowed area gets further reduced in size, owing to the precision of the KamLAND data. For all the panels the precision on the range of allowed value of Δm_{21}^2 is seen to improve, however there is little improvement in the precision of $\sin^2 \theta_{12}$ [23] (see also [27]). In the last row of Figure 8 we get a glimpse of the scenario that

would show itself if the future KamLAND data conforms to a point in the high-LMA zone. Since the low-LMA is now strongly favored over high-LMA by the global solar neutrino data, if such a contradictory situation arises whereby KamLAND would favor high-LMA, then both the solution would get allowed and the ambiguity would remain. However as can be seen in the last row panels of Figure 8, the best-fit still comes in the low-LMA.

6 Conclusions

We analysed the impact of the salt phase data from SNO in global solar neutrino oscillation analysis, including the KamLAND data as well. The inclusion of the CC and NC event rates from the SNO salt phase data firmly establishes Δm_{21}^2 to lie in the low-LMA region. Values of Δm_{21}^2 in the LOW region get disfavoured at more than 3σ just from global solar data, and at almost 5σ from the combined solar and KamLAND data. The combined effect of the SNO spectrum data from the D_2O phase and of the data from the salt phase results in lowering the upper bound on Δm_{21}^2 to $\Delta m_{21}^2 \leq 1.7 \times 10^{-4}$ eV 2 (99.73% C.L.). The global solar + KamLAND data still admit the high-LMA solution, but it appears only at 3σ level. The addition of the new SNO data restricts the mixing angle θ_{12} from above and maximal mixing is now excluded at more than 5σ . With the inclusion of non-zero values of the mixing angle θ_{13} in a 3-neutrino mixing analysis, the allowed regions in the $\Delta m_{21}^2 - \sin^2 \theta_{12}$ plane decrease in size as θ_{13} increases. At $\sin^2 \theta_{13} \geq 0.075$ no allowed regions are obtained at 99.73% C.L. The solution due to transitions into sterile neutrino is excluded at 7.8σ with the salt data. However, solar ν_e transitions into a mixed sterile + active state are allowed, with the sterile fraction restricted to be $< 52\%$ at 3σ . With the knowledge of mass and mixing angles becoming more precise, the predicted ranges for the day-night asymmetry in SK and SNO and of the rates in Borexino and the LowNU experiments narrow down. We also studied the impact of prospective KamLAND data statistics increase to 1 kton for the determination of the solar neutrino oscillation parameters. If the spectrum is simulated at a point in the low-LMA region, the allowed 3σ area in the high-LMA zone reduces in size. If, however, the KamLAND spectrum corresponds to a point in the high-LMA zone, the conflicting trend of solar and KamLAND data would make the high-LMA zone reappear at 90% C.L. and the determination of Δm_{21}^2 would remain ambiguous.

S.G. would like to thank The Abdus Salam International Centre for Theoretical Physics for hospitality.

References

- [1] S. N. Ahmed *et al.* [SNO Collaboration], arXiv:nucl-ex/0309004.
- [2] B. T. Cleveland *et al.*, *Astrophys. J.* **496**, 505 (1998); J. N. Abdurashitov *et al.* [SAGE Collaboration], arXiv:astro-ph/0204245; W. Hampel *et al.* [GALLEX Collaboration], *Phys. Lett. B* **447**, 127 (1999); E. Bellotti, Talk at Gran Sasso National Laboratories, Italy, May 17, 2002;

T. Kirsten, talk at *Neutrino 2002*, XXth International Conference on Neutrino Physics and Astrophysics, Munich, Germany, May 25-30, 2002. (<http://neutrino2002.ph.tum.de/>)

- [3] S. Fukuda *et al.* [Super-Kamiokande Collaboration], *Phys. Lett. B* **539**, 179 (2002) [arXiv:hep-ex/0205075].
- [4] Q. R. Ahmad *et al.* [SNO Collaboration], *Phys. Rev. Lett.* **87**, 071301 (2001) [arXiv:nucl-ex/0106015].
- [5] Q. R. Ahmad *et al.* [SNO Collaboration], *Phys. Rev. Lett.* **89**, 011301 (2002) [arXiv:nucl-ex/0204008]. Q. R. Ahmad *et al.* [SNO Collaboration], *Phys. Rev. Lett.* **89**, 011302 (2002) [arXiv:nucl-ex/0204009];
- [6] L. Wolfenstein, *Phys. Rev. D* **17**, 2369 (1978) ; S. P. Mikheev and A. Y. Smirnov, *Sov. J. Nucl. Phys.* **42** (1985) 913 [*Yad. Fiz.* **42**, 1441 (1985)] ; S. P. Mikheev and A. Y. Smirnov, *Sov. J. Nucl. Phys.* **42** (1985) 913 [*Yad. Fiz.* **42**, 1441 (1985)] ; S. P. Mikheev and A. Y. Smirnov, *Nuovo Cim. C* **9**, 17 (1986).
- [7] A. Bandyopadhyay, S. Choubey, S. Goswami and K. Kar, *Phys. Lett. B* **519**, 83 (2001) [arXiv:hep-ph/0106264].
- [8] A. Bandyopadhyay, S. Choubey, S. Goswami and D. P. Roy, *Phys. Lett. B* **540**, 14 (2002) [arXiv:hep-ph/0204286]. S. Choubey, A. Bandyopadhyay, S. Goswami and D. P. Roy, arXiv:hep-ph/0209222.
- [9] K. Eguchi *et al.* [KamLAND Collaboration], *Phys. Rev. Lett.* **90**, 021802 (2003) [arXiv:hep-ex/0212021].
- [10] A. Bandyopadhyay, S. Choubey, R. Gandhi, S. Goswami and D. P. Roy, *Phys. Lett. B* **559**, 121 (2003) [arXiv:hep-ph/0212146];
- [11] G. L. Fogli *et al.*, *Phys. Rev. D* **67**, 073002 (2003) [arXiv:hep-ph/0212127]; M. Maltoni, T. Schwetz and J. W. Valle, arXiv:hep-ph/0212129; J. N. Bahcall, M. C. Gonzalez-Garcia and C. Pena-Garay, *JHEP* **0302**, 009 (2003) [arXiv:hep-ph/0212147]; H. Nunokawa, W. J. Teves and R. Zukanovich Funchal, arXiv:hep-ph/0212202; P. Aliani *et al.*, arXiv:hep-ph/0212212; P. C. de Holanda and A. Y. Smirnov, *JCAP* **0302**, 001 (2003) [arXiv:hep-ph/0212270].
- [12] M. Apollonio *et al.*, *Phys. Lett. B* **466** (1999) 415; F. Boehm *et al.*, *Phys. Rev. D* **62** (2000) 072002.
- [13] S.M. Bilenky, D. Nicolo and S.T. Petcov, *Phys. Lett. B* **538** (2002) 77.
- [14] Super-Kamiokande Coll., Y. Hayato *et al.*, Talk given at the Int. EPS Conference on High Energy Physics, July 17 - 23, 2003, Aachen, Germany.
- [15] [Super-Kamiokande Collaboration], arXiv:hep-ex/0309011.

- [16] “HOWTO use the SNO Salt Flux Results”, and “HOWTO use the SNO Solar Neutrino Spectral data”, SNO Collaboration, <http://www.sno.phy.queensu.ca/>;
- [17] M. Maris and S. T. Petcov, Phys. Lett. B **534** (2002) 17 [arXiv:hep-ph/0201087], and Phys. Rev. D62 (2000) 093006 (arXiv:hep-ph/0003301).
- [18] S.T. Petcov, Phys. Lett. B **200**, 373 (1988), and Phys. Lett. B **214**, 139 (1988); S.T. Petcov and J. Rich, Phys. Lett. B **224**, 401 (1989); P.I. Krastev and S.T. Petcov, Phys. Lett. B **207**, 64 (1988); E. Lisi et al., Phys. Rev. D **63**, 093002 (2000).
- [19] C. Athanassopoulos *et al.*, (The LSND Collaboration) Phys. Rev. Lett. **77**, 3082 (1996); C. Athanassopoulos *et al.*, (The LSND Collaboration) Phys. Rev. Lett. **81**, 1774 (1998).
- [20] J. Formaggio, talk at *5th International Workshop on Neutrino Factories & Superbeams*, NuFact '03, Columbia University, New York, 5-11 June 2003; <http://www.cap.bnl.gov/nufact03>.
- [21] G. Alimonti *et al.* [Borexino Collaboration], Astropart. Phys. **16**, 205 (2002) [arXiv:hep-ex/0012030].
- [22] S. Schönert, talk at Neutrino 2002, Munich, Germany, (<http://neutrino2002.ph.tum.de>).
- [23] A. Bandyopadhyay, S. Choubey and S. Goswami, Phys. Rev. D **67**, 113011 (2003) [arXiv:hep-ph/0302243].
- [24] J. N. Bahcall and C. Pena-Garay, arXiv:hep-ph/0305159.
- [25] A. Bandyopadhyay, S. Choubey, R. Gandhi, S. Goswami and D. P. Roy, arXiv:hep-ph/0211266.
- [26] V. D. Barger, D. Marfatia and B. P. Wood, Phys. Lett. B **498**, 53 (2001) [arXiv:hep-ph/0011251]; H. Murayama and A. Pierce, Phys. Rev. D **65**, 013012 (2002) [arXiv:hep-ph/0012075]; A. de Gouvea and C. Pena-Garay, Phys. Rev. D **64**, 113011 (2001) [arXiv:hep-ph/0107186].
- [27] S. Choubey, S. T. Petcov and M. Piai, arXiv:hep-ph/0306017.